



# Simulating the effect of cerebral blood flow changes on regional quantification of [<sup>18</sup>F]flutemetamol and [<sup>18</sup>F]florbetaben studies

Fiona Heeman<sup>1</sup> , Maqsood Yaqub<sup>1</sup>, Isadora Lopes Alves<sup>1</sup>, Kerstin Heurling<sup>2</sup> , Santiago Bullich<sup>3</sup>, Juan D Gispert<sup>4,5,6</sup>, Ronald Boellaard<sup>1</sup>, Adriaan A Lammertsma<sup>1</sup> and on behalf of the AMYPAD Consortium

## Abstract

Global and regional changes in cerebral blood flow (CBF) can result in biased quantitative estimates of amyloid load by PET imaging. Therefore, the current simulation study assessed effects of these changes on amyloid quantification using a reference tissue approach for [<sup>18</sup>F]flutemetamol and [<sup>18</sup>F]florbetaben. Previously validated pharmacokinetic rate constants were used to simulate time-activity curves (TACs) corresponding to full dynamic and dual-time-window acquisition protocols. CBF changes were simulated by varying the tracer delivery ( $K_1$ ) from +25 to –25%. The standardized uptake value ratio (SUVr) was computed and TACs were fitted using reference Logan (RLogan) and the simplified reference tissue model (SRTM) to obtain the relative delivery rate ( $R_1$ ) and volume of distribution ratio (DVR). RLogan was least affected by CBF changes ( $\chi^2 = 583$   $p < 0.001$ ,  $\chi^2 = 81$   $p < 0.001$ , for [<sup>18</sup>F]flutemetamol and [<sup>18</sup>F]florbetaben, respectively) and the extent of CBF sensitivity generally increased for higher levels of amyloid. Further, SRTM-derived  $R_1$  changes correlated well with simulated CBF changes ( $R^2 > 0.95$ ) and SUVr's sensitivity to CBF changes improved for later uptake-times, with the exception of [<sup>18</sup>F]flutemetamol cortical changes. In conclusion, RLogan is the preferred method for amyloid quantification of [<sup>18</sup>F]flutemetamol and [<sup>18</sup>F]florbetaben studies and SRTM could be additionally used for obtaining a CBF proxy.

## Keywords

Alzheimer's disease, amyloid PET, cerebral blood flow, quantification, simulation study

Received 7 November 2019; Revised 24 February 2020; Accepted 15 March 2020

## Introduction

Amyloid-beta accumulation ( $A\beta$ ) in the brain is one of the hallmarks of Alzheimer's disease (AD). It can be visualised and quantified using positron emission tomography (PET) and both static or dynamic scanning protocols can be used.<sup>1,2</sup> The static protocol has the advantage of a short scan duration together with relatively simple processing and analytical steps, while the dynamic protocol provides higher accuracy at the cost of a much longer scan, more complex processing and advanced kinetic analysis. The semi-quantitative parameter obtained from a static scan, the standardized uptake value ratio (SUVr), depends on post-injection starting time and duration of the acquisition, and may be affected by changes in cerebral blood flow (CBF) as demonstrated for [<sup>11</sup>C]PiB.<sup>3–6</sup> In contrast, the non-displaceable binding potential ( $BP_{ND}$ ), derived

from a dynamic PET scan, is less sensitive to noise, more robust against CBF changes, and for [<sup>11</sup>C]PiB it has been shown to be the parameter of choice when

<sup>1</sup>Amsterdam UMC, Vrije Universiteit Amsterdam, Radiology and Nuclear Medicine, Amsterdam Neuroscience, Amsterdam, Netherlands

<sup>2</sup>Antaros Medical AB, Mölndal, Sweden

<sup>3</sup>Life Molecular Imaging GmbH, Berlin, Germany

<sup>4</sup>Barcelonaβeta Brain Research Centre, Pasqual Maragall Foundation, Barcelona, Spain

<sup>5</sup>Centro de Investigación Biomédica en Red de Bioingeniería, Biomateriales y Nanomedicina (CIBER-BBN), Madrid, Spain

<sup>6</sup>Department of Experimental and Health Sciences, Universitat Pompeu Fabra, Barcelona, Spain

## Corresponding author:

Fiona Heeman, Amsterdam UMC, locatie VUmc, De Boelelaan 1117, Amsterdam 1081 HV, Netherlands.  
Email: f.heeman@amsterdamumc.nl

measuring longitudinal changes in amyloid burden.<sup>5,6</sup> This characteristic may be especially important in situations where changes in CBF can occur, such as when measuring disease progression or treatment response in clinical trials. As a compromise between the protocols mentioned above, dynamic data acquisitions from a dual-time-window protocol have gained attention, in which data are acquired separately for early and late phases of tracer uptake to reduce overall scanning time, maintain high quantitative accuracy and provide tracer delivery information.<sup>7,8</sup>

Cerebral blood flow declines with age and differs per brain region.<sup>9</sup> Compared with young adults (25 years), elderly (late 70s) can present with up to 25% CBF reductions, with an average annual CBF decline in grey matter of approximately 0.5%.<sup>9,10</sup> On top of this global decline, day-to-day whole brain CBF fluctuations of around 30% have been reported in test–retest studies; however, this percentage was assumed to consist of both physiological as well as measurement error.<sup>11</sup> Furthermore, drugs may also exert an effect on CBF,<sup>12,13</sup> thus potentially compromising the measurement of amyloid changes associated to pharmacological interventions. In the context of AD, additional relative CBF changes may be present, as focal reductions in CBF have been observed in several brain regions.<sup>14–16</sup> A study on non-demented older adults scanned with [<sup>11</sup>C]PiB showed that subjects with elevated [<sup>11</sup>C]PiB signals experienced greater relative CBF variations, mainly in those regions showing increased amyloid deposition.<sup>17</sup> Given that CBF differs per region, declines with age, and that additional regional CBF changes occur during the course of Alzheimer's disease, it is important to assess whether and, if so, to which extent these changes affect quantification of amyloid load. Furthermore, the additional effects of acquisition start-time and duration on quantitative accuracy need to be understood, due to its relevance in clinical and research practice.<sup>3</sup>

The effect of CBF changes on amyloid load quantification has been assessed previously for [<sup>11</sup>C]PiB, [<sup>18</sup>F]florbetaben and semi-quantitative measures of [<sup>18</sup>F]florbetapir.<sup>5,7,18</sup> These studies showed that large cortical CBF reductions resulted in a maximum change of  $\pm 10\%$  in SUVR. For large global CBF reductions, a larger bias was observed for [<sup>11</sup>C]PiB as compared with [<sup>18</sup>F]florbetaben and [<sup>18</sup>F]florbetapir.<sup>5,7,18</sup> These differences between tracer differences are to be expected due to differences in tracer kinetics and corresponding equilibrium times. However, the effect of CBF changes on quantification of [<sup>18</sup>F]flutemetamol scans remains unknown, just as the potential effects of such changes on novel dual-time-window protocols. Therefore, the present simulation study aimed to assess the effects of regional (i.e. target and reference tissues) and global

CBF changes on quantitative amyloid measures derived from static, dynamic and dual-time window scanning protocols using reference tissue approaches,<sup>8</sup> thereby focusing on [<sup>18</sup>F]flutemetamol and [<sup>18</sup>F]florbetaben, the two tracers used within the AMYPAD consortium. A second aim was to assess whether the relative delivery rate ( $R_1$ ) of both ligands could be used to accurately monitor changes in CBF.<sup>16,19</sup>

## Materials and methods

### Subjects and PET data

Previously reported clinical PET data from 6 [<sup>18</sup>F]flutemetamol and 20 [<sup>18</sup>F]florbetaben subjects (both control and AD subjects), consisting of regional time-activity curves (TACs) and whole blood and/or plasma input curves, were used for this simulation study.<sup>20,21</sup> All participants provided written informed consent in accordance with the Declaration of Helsinki. The Ethical Committee of the University Hospitals Leuven approved the study protocol for the [<sup>18</sup>F]flutemetamol study (EudraCT 2007-000784-19, Registered 8 February 2007). For [<sup>18</sup>F]florbetaben, the local Institutional Review Board of University of Leipzig, the National Radiation Safety Committee, and the German Federal Institute for Drugs and Medical Devices approved the study protocol (EudraCT 2006-003882-15, Registered 2006). The first group received a bolus injection ( $<40$  s) of  $181 \pm 5$  MBq [<sup>18</sup>F]flutemetamol and were scanned on a Siemens HiRez Biograph 16 PET/CT scanner.<sup>3,20</sup> The second group received an injection of  $300 \pm 60$  MBq [<sup>18</sup>F]florbetaben (over 90 s) and were scanned on a ECAT HR+ Siemens/CTI scanner.<sup>21</sup> As described previously, whole blood curves and metabolite-corrected plasma input curves were available for [<sup>18</sup>F]flutemetamol, and metabolite-corrected plasma input curves and discrete whole blood samples for [<sup>18</sup>F]florbetaben.<sup>8</sup> Subsequently, regional TACs were fitted using the reversible two-tissue compartment model (four rate constants) with additional blood volume fraction parameter ( $2T4k\_V_b$ ) to obtain pharmacokinetic rate constants for the target (composite cortical region consisting of anterior and posterior cingulate, frontal, parietal, and lateral and medialtemporal cortex) and reference tissue (grey matter cerebellum).<sup>8</sup>

### TAC simulations

Based on the pharmacokinetic rate constants estimated from the clinical data mentioned above, realistic target and reference tissue TACs of 130 min duration were simulated using the  $2T4k\_V_b$  model (see Figure 1 and Table 1 for the rate constants).<sup>8</sup> Target tissue TACs

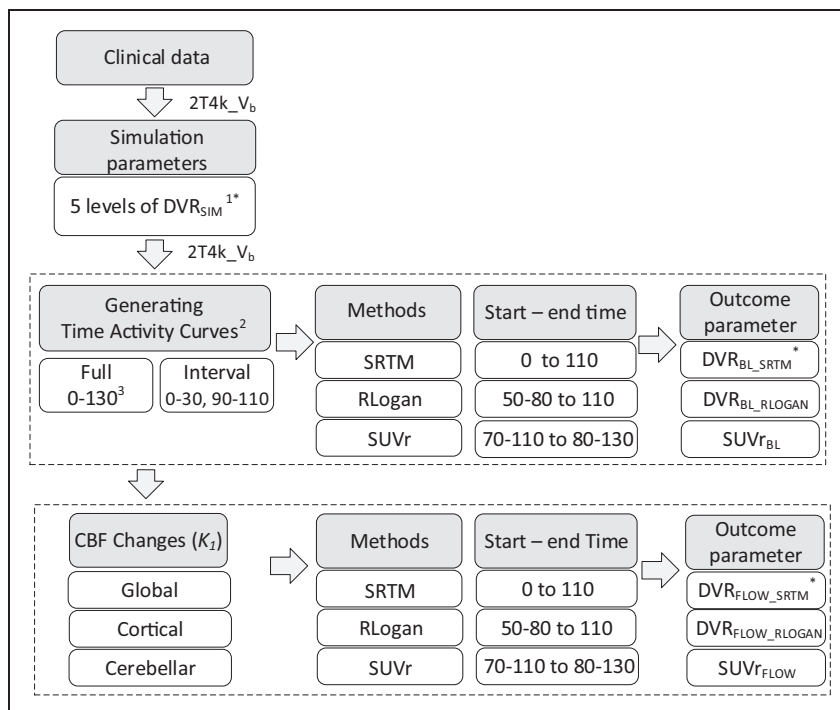


**Figure 1.** Schematic overview of the applied methods. 1. [ $^{18}F$ ]flutemetamol  $DVR_{SIM}$  (simulated volume of distribution ratio) ranged from 1.022 to 1.778, [ $^{18}F$ ]florbetaben  $DVR_{SIM}$  ranged from 1.026 to 2.051. 2. All steps were repeated for 1 and 2% noise. 3. All values are minutes post injection (p.i.). \*Here  $DVR$  refers to  $BP_{ND}+1$ . Abbreviations:  $V_b$ : blood volume; BL: baseline (no cerebral blood flow change); SRTM: simplified reference tissue model; RLOGAN: reference Logan, SUVr: standardised uptake value ratio; FLOW: with changes in cerebral blood flow.

**Table 1.** Rate constants used for CBF simulations.

	Global		Local cortical		Local cerebellar	
	Target	Reference	Target	Reference	Target	Reference
<b>[<math>^{18}F</math>]flutemetamol</b>						
$K_1$	0.186–0.310	0.240–0.400	0.186–0.310	0.320 <sup>a</sup>	0.248 <sup>a</sup>	0.240–0.400
$k_2$	0.060–0.100	0.077–0.129	0.060–0.010	0.103 <sup>a</sup>	0.080 <sup>a</sup>	0.077–0.129
$k_3$	0.008–0.028	0.018	0.008–0.028	0.018	0.008–0.028	0.018
$k_4$	0.020	0.050	0.020	0.050	0.020	0.050
<b>[<math>^{18}F</math>]florbetaben</b>						
$K_1$	0.170–0.283	0.188–0.313	0.170–0.283	0.250 <sup>a</sup>	0.226 <sup>a</sup>	0.188–0.313
$k_2$	0.052–0.087	0.057–0.095	0.052–0.087	0.076 <sup>a</sup>	0.069 <sup>a</sup>	0.057–0.095
$k_3$	0.010–0.030	0.007	0.010–0.030	0.007	0.010–0.030	0.007
$k_4$	0.010	0.007	0.010	0.007	0.010	0.007

<sup>a</sup>Baseline parameter, corresponding to a 0% CBF change. Units:  $K_1$  in  $ml \times g^{-1} \times min^{-1}$  and  $k_2$  in  $min^{-1}$ .

Note: For both tracers, the blood volume fraction parameter ( $V_b$ ) was set to 0.05.

were simulated for a clinically observed range of  $BP_{ND}$  values (captured by five simulated  $BP_{ND}$  values, Figure 1), and noise (0, 1 and 2%) corresponding to regions of interest (ROI) of various sizes was added to the target tissue TACs.<sup>22</sup> This resulted in a total of 50 TACs per noise level (identical TACs in case of 0% noise) and for each simulated  $BP_{ND}$  (see Figure 1 for a

flowchart of the method). No noise was added to reference tissue TACs due to its relatively large volume.

### Simulating CBF changes

Given that the rate constant for tracer delivery ( $K_1$ ) can be considered a proxy for blood flow as long as the

extraction remains constant ( $K_1 = \text{Flow} \times \text{Extraction}$ ), changes in CBF were simulated by varying both  $K_1$  and tissue clearance ( $k_2$ ), in order to maintain the non-displaceable volume of distribution constant ( $V_{ND} = K_1/k_2$ ).<sup>23</sup> Both increases and decreases were simulated (from +25 to -25%) in three different scenarios (see Table 1 and Figure 2 for the simulation parameters and a schematic overview of the simulations):

1. Global CBF changes: equal variations in  $K_1$  and  $k_2$  for target and reference tissues.
2. Cortical CBF changes: variations in  $K_1$  and  $k_2$  only for the target tissue, reference tissue parameters were kept constant.
3. Cerebellar CBF changes: variations in  $K_1$  and  $k_2$  only for the reference tissue, target tissue parameters were kept constant.

### Dual-time-window TACs

In addition to the full 130 min TACs, dual-time-window TACs (here called ‘interval TACs’) were created by removing data points from target and reference tissue TACs according to the dual-time-window protocol.<sup>8</sup> In short, the first 110 min were used (corresponding to a dynamic scanning protocol) and data points between the early (0–30 min post injection (p.i.)) and late acquisition phase (90–110 min p.i.) were deleted.

### Estimating parameters of interest

SUVr was calculated from the 130 min full TACs, for starting times ( $t^*$ ) ranging from 70 to 110 min p.i. (interval  $t^*$ :  $3 \times 5$  min,  $4 \times 2.5$  min,  $3 \times 5$  min), and durations of 10, 15 and 20 min. Next, 110 min of the full TACs (corresponding to a dynamic scanning protocol) and interval TACs were fitted using reference Logan

(RLogan) to estimate the volume of distribution ratio (DVR).<sup>24</sup> The implementation of this model did not require fixing  $k_2'$  (as per equation (7)).<sup>24</sup> The linearization start times ( $t^*$ ) evaluated ranged from 50 to 80 min p.i. (in steps of 10 min) and interpolation of interval target tissue TACs was performed using cubic interpolation, as the method is routinely used for parametric imaging. Finally, 110 min of the full TACs and the interval TACs were fitted using the simplified reference tissue model (SRTM) to estimate  $R_1$ ,  $k_2$  and  $BP_{ND}$ .<sup>25</sup> Given that SRTM requires a continuous input to fit the target tissue TACs, missing data points of the reference tissue interval TACs were interpolated using the 2T4k\_V<sub>b</sub> model together with a typical, tracer specific input function as validated previously.<sup>8</sup> In addition, for both tracers, boundary values (optimized for full, noiseless TACs) were set for all kinetic parameters to prevent physiologically implausible results (Supplementary Figure 1). Optimal boundaries were defined based on the simulated parameter range and lower boundaries were fine-tuned (based on parameter histograms) in case of  $k_2$ . This procedure selected the boundary value that resulted in least bias (calculated from the simulated  $BP_{ND}+1$ ) across CBF scenarios and amyloid binding levels

### Statistical analysis

For all analyses (i.e. all amyloid levels, starting times, durations, scanning protocols and for TACs both with and without noise), parameter estimates obtained in the absence of CBF variations were used as baseline parameters ( $SUV_{r\_BL}$ ,  $R_{1\_BL}$ ,  $DVR_{BL\_SRTM}$  and  $DVR_{BL\_RLOGAN}$ , Table 1). Next, percentage change as a result of CBF variations was calculated relative to each baseline for  $SUV_{r\_FLOW}$ ,  $R_{1\_FLOW}$ ,  $DVR_{FLOW\_SRTM}$  and  $R_{Logan} DVR_{FLOW\_RLOGAN}$ :

$$\Delta PAR_{FLOW} (\%) = \frac{PAR_{FLOW} - PAR_{BL}}{PAR_{BL}} \cdot 100\%$$

where PAR corresponds to the parameter of interest (i.e. SUVr, DVR or  $R_1$ ). These parameters were then used to assess the sensitivity of the methods to variations in CBF. This was done for different levels of amyloid load, different scanning protocols, noise levels and uptake times.

Non-parametric Kruskal–Wallis tests were used to assess differences in sensitivity to CBF variations between methods and simulated  $BP_{ND}$  values.<sup>26</sup> In addition, the maximum percentage change due to CBF variations was compared between methods and for the whole spectrum of simulated  $BP_{ND}$  values. Furthermore, to assess the relationship between  $\Delta R_{1\_FLOW}$  and simulated  $\Delta CBF$ , the coefficient of

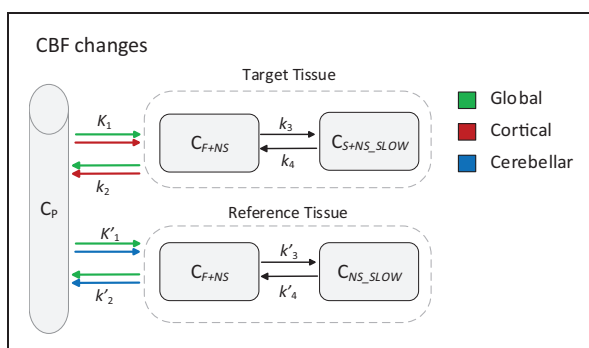


**Figure 2.** Schematic overview of the simulated CBF changes.  $C_p$ : tracer plasma radioactivity concentration,  $C_{F+NS}$ : free and non-specifically bound concentration in tissue,  $C_{S+NS\_SLOW}$ : specifically bound and slow non-specifically bound concentration in tissue, all units  $Bq \cdot ml^{-1}$ . Units of the rate constants:  $K_1$  in  $ml \times g^{-1} \times min^{-1}$  and  $k_2, k_3, k_4$  in  $min^{-1}$ .

determination ( $R^2$ ) was calculated based on Pearson's correlation coefficient. Next, differences in sensitivity were compared between full and interval TACs fitted with SRTM and RLogan using the post hoc Mann–Whitney U test and boxplot analyses, where outliers were defined as points outside the whiskers (created using the Tukey method<sup>27</sup>). Subsequently, effects of noise on sensitivity to CBF changes and its relationship with all parameters were evaluated based on boxplot analyses. Finally, using Kruskal–Wallis tests, effects of altering starting times ( $t^*$ ) on CBF sensitivity were evaluated for RLogan and altering starting times and acquisition duration on CBF sensitivity for SUVr.

## Results

### Evaluation of outcome parameter(s)

The resulting boundary values for [<sup>18</sup>F]flutemetamol were:  $R_1$ : lower boundary (LB) = 1e-6 upper boundary (UB) = 2.00,  $k_2$ : LB = 0.018 UB = 2.00,  $BP_{ND}$ : LB = -0.50 UB = 5.00. For [<sup>18</sup>F]florbetaben, boundary

values were:  $R_1$ : LB = 1e-6 UB = 2.00,  $k_2$ : LB = 0.028 UB = 2.00,  $BP_{ND}$ : LB = -0.50 UB = 5.00.

### Sensitivity to CBF changes – Comparison between methods

[<sup>18</sup>F]flutemetamol. Overall,  $DVR_{FLOW_{RLOGAN}}$  was least sensitive to changes in CBF ( $\chi^2 = 583$ ,  $p < 0.001$ ). With respect to global CBF changes, all models showed less than 6% change. More specifically,  $DVR_{FLOW_{SRTM}}$  showed least overall sensitivity to global CBF changes ( $\chi^2 = 72$ ,  $p < 0.001$ ), while  $DVR_{FLOW_{RLOGAN}}$  showed the smallest maximum change (3.7%) followed by  $SUVr_{FLOW}$  (5.1%) and  $DVR_{FLOW_{SRTM}}$  (max. 5.8%). For cortical and cerebellar changes,  $DVR_{FLOW_{RLOGAN}}$  was least sensitive to CBF changes ( $\chi^2 = 995$ ,  $p < 0.001$ , maximum regional change: 2.0% compared with  $DVR_{FLOW_{SRTM}}$  13.4% and  $SUVr_{FLOW}$  4.8%), as shown in Figure 3. Sensitivity to simulated CBF changes increased for higher simulated levels of amyloid load for global ( $DVR_{FLOW_{SRTM}}$ :  $\chi^2 = 280$ ,  $p < 0.001$ ;  $DVR_{FLOW_{RLOGAN}}$ :  $\chi^2 = 104$ ,  $p < 0.001$ ;  $SUVr_{FLOW}$ :  $\chi^2 = 239$ ,  $p < 0.001$ ), cortical ( $DVR_{FLOW_{SRTM}}$ :  $\chi^2 = 63$ ,  $p < 0.001$ ;  $DVR_{FLOW_{RLOGAN}}$ :  $\chi^2 = 118$ ,  $p < 0.001$ ;  $SUVr_{FLOW}$ :  $\chi^2 = 142$ ,  $p < 0.001$ ) and cerebellar changes

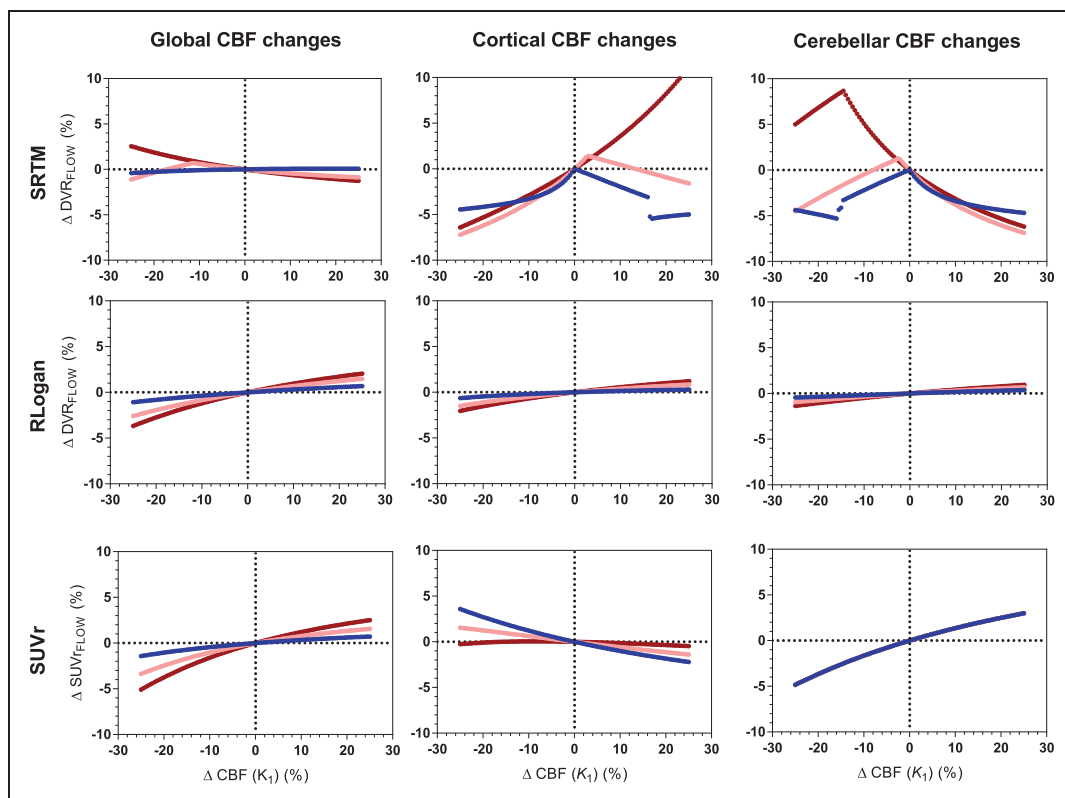


**Figure 3.** [<sup>18</sup>F]flutemetamol: sensitivity to CBF changes across methods for three levels of amyloid load. Low amyloid (blue):  $DVR = 1.022$ , intermediate amyloid (pink):  $DVR = 1.400$ , high amyloid (red):  $DVR = 1.778$ . Four values (between 10 and 10.6%) for SRTM cortical CBF changes high amyloid are not shown. RLogan linearization time was 50–110 min p.i., SUVr uptake time was 90–110 min p.i.

( $DVR_{FLOW_{SRTM}}$ :  $\chi^2 = 161$ ,  $p < 0.001$ ;  $DVR_{FLOW_{RLOGAN}}$ :  $\chi^2 = 92$ ,  $p < 0.001$ ;  $SUV_{FLOW}$ : no significant difference).

**[ $^{18}F$ ]florbetaben.** Overall,  $DVR_{FLOW_{RLOGAN}}$  was least sensitive to CBF changes compared with the other methods ( $\chi^2 = 81$ ,  $p < 0.001$ ), in particular for cerebellar changes ( $\chi^2 = 457$ ,  $p < 0.001$ ), and showed smallest maximum change ( $DVR_{FLOW_{RLOGAN}}$ : 1.2%,  $DVR_{FLOW_{SRTM}}$ : 6.1%,  $SUV_{FLOW}$ : 2.4%). With respect to global CBF changes, all methods showed a very similar sensitivity pattern with CBF decreases resulting in lower and CBF increases in higher changes (maximum change:  $DVR_{FLOW_{RLOGAN}}$ : 5.2%,  $DVR_{FLOW_{SRTM}}$ : 7.5% and  $SUV_{FLOW}$ : 6.1%), as shown in Figure 4. With respect to cortical CBF changes,  $SUV_{FLOW}$  was least sensitive ( $\chi^2 = 68$ ,  $p < 0.001$ ) and showed the smallest maximum change ( $SUV_{FLOW}$ : 3.7%,  $DVR_{FLOW_{RLOGAN}}$ : 4.7% and  $DVR_{FLOW_{SRTM}}$ : 7.3%). Furthermore, in general, the extent of CBF sensitivity increased for higher levels of simulated amyloid load, for global ( $DVR_{FLOW_{SRTM}}$ :  $\chi^2 = 290$ ,  $p < 0.001$ ;  $DVR_{FLOW_{RLOGAN}}$ :  $\chi^2 = 171$ ,  $p < 0.001$ ;  $SUV_{FLOW}$ :  $\chi^2 = 274$ ,  $p < 0.001$ ), cortical ( $DVR_{FLOW_{SRTM}}$ :  $\chi^2 = 131$ ,  $p < 0.001$ ;  $DVR_{FLOW_{RLOGAN}}$ :  $\chi^2 = 105$ ,  $p < 0.001$ ;  $SUV_{FLOW}$ :  $\chi^2 = 184$ ,  $p < 0.001$ ) and cerebellar changes ( $DVR_{FLOW_{SRTM}}$ :  $\chi^2 = 13$ ,  $p = 0.011$ ;  $DVR_{FLOW_{RLOGAN}}$ :  $\chi^2 = 201$ ,  $p < 0.001$ ;  $SUV_{FLOW}$ : no significant difference).

**Relative delivery and CBF changes.** For [ $^{18}F$ ]flutemetamol, correlations between simulated  $\Delta CBF$  and  $\Delta R_{1\_FLOW}$  were high for all amyloid levels both for cortical ( $R^2 = 0.98$  to  $1.00$ ,  $p < 0.001$ ) as well as cerebellar CBF changes ( $R^2 = 0.97$  to  $1.00$ ,  $p < 0.001$ ). For [ $^{18}F$ ]florbetaben, high correlations were also observed between simulated  $\Delta CBF$  and  $\Delta R_{1\_FLOW}$  across amyloid levels both for cortical ( $R^2 = 0.98$  to  $0.99$ ,  $p < 0.001$ ) and cerebellar CBF changes ( $R^2 = 0.95$  to  $0.99$ ,  $p < 0.001$ ). Very similar results were obtained for  $R_1$  estimates derived from interval TACs (data not shown).

**Sensitivity to CBF changes – Full versus interval TACs.** For [ $^{18}F$ ]florbetaben, full TACs were found to be less sensitive to CBF changes than interval TACs ( $p < 0.001$ ), while for [ $^{18}F$ ]flutemetamol, the opposite effect was found ( $p < 0.001$ ). Post hoc tests revealed that for [ $^{18}F$ ]florbetaben this effect was present for both models, while for [ $^{18}F$ ]flutemetamol the effect was only present for SRTM. Furthermore, for both tracers, most outliers were present for interval compared to full TACs (outliers interval TACs: [ $^{18}F$ ]flutemetamol: 91.67%, [ $^{18}F$ ]florbetaben: 66.67%). These outliers were only observed for TACs fitted with SRTM, predominantly corresponding to low simulated amyloid levels (Figure 5). For [ $^{18}F$ ]florbetaben, interval TAC-

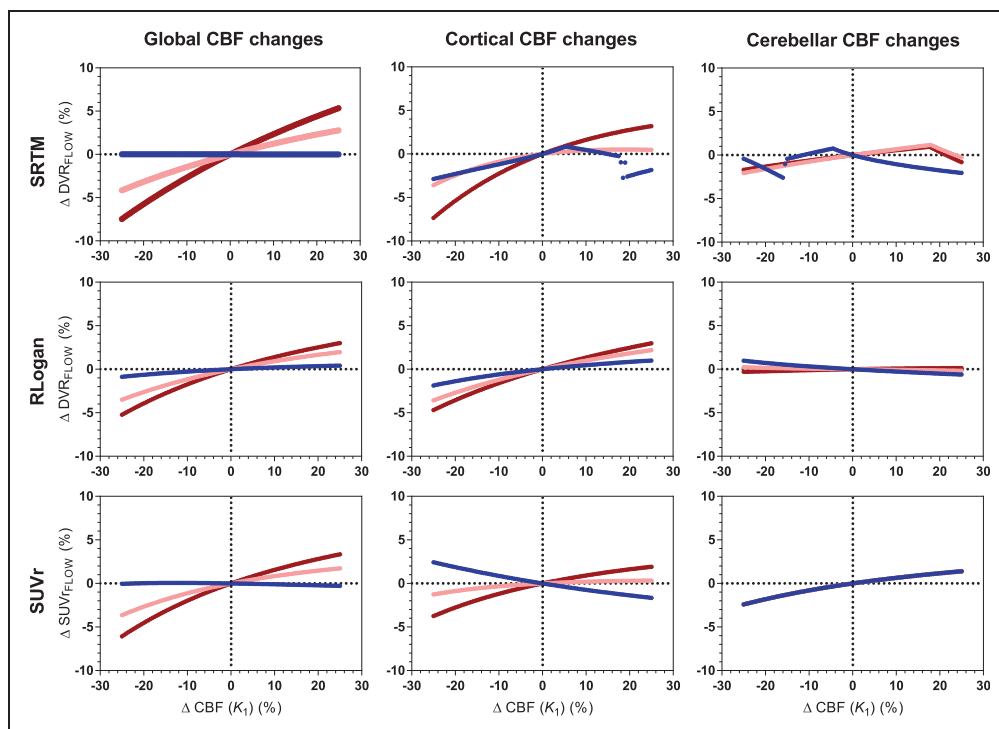


**Figure 4.** [ $^{18}F$ ]florbetaben: sensitivity to CBF changes across methods for three levels of amyloid load. Low amyloid (blue):  $DVR = 1.026$ , intermediate amyloid (pink):  $DVR = 1.538$ , high amyloid (red):  $DVR = 2.051$ . RLogan linearization time was 50–110 min p.i., SUVr uptake time was 90–110 min p.i.

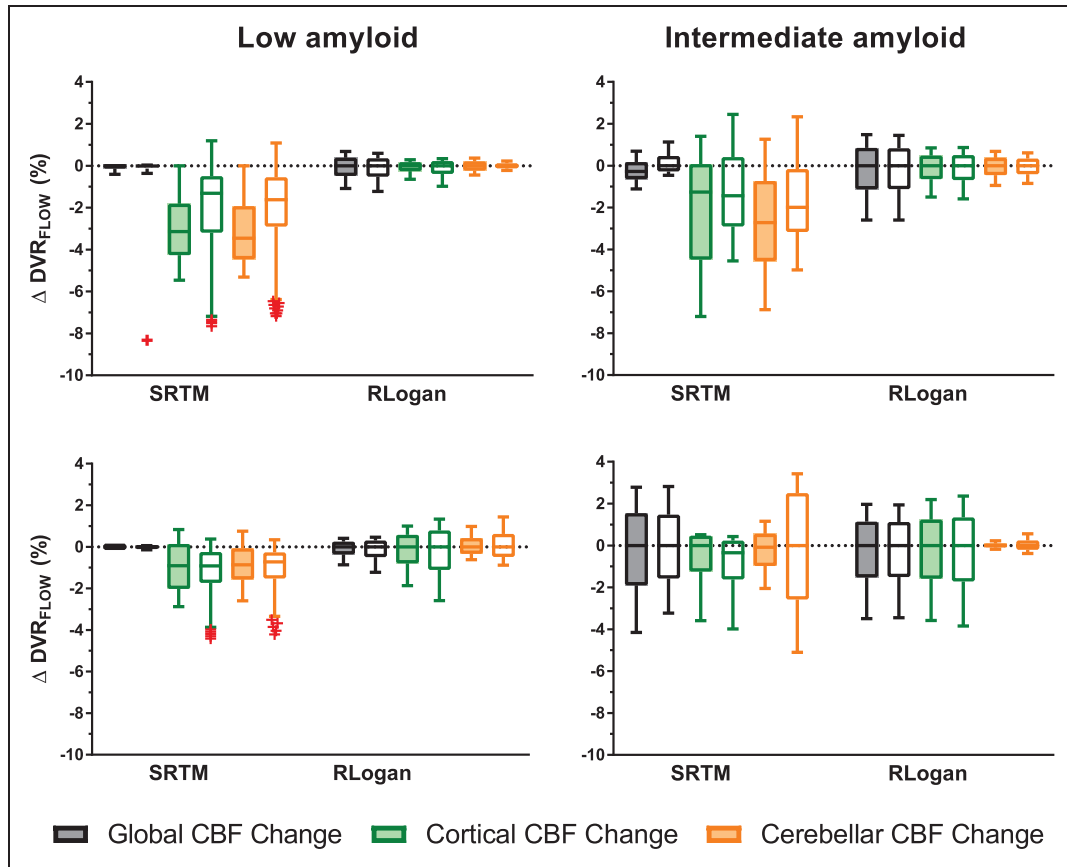


**Figure 5.** Comparison of full and interval TACs and their sensitivity to CBF changes. Coloured boxes represent full- and uncoloured boxes interval TACs. Upper row [ $^{18}\text{F}$ ]flutemetamol, bottom row [ $^{18}\text{F}$ ]florbetaben. Note: whiskers were defined according to the Tukey method and outliers are depicted as red crosses.

derived  $\text{DVR}_{\text{FLOW}_{\text{SRTM}}}$  was more sensitive to cerebellar CBF changes compared to full TAC-derived  $\text{DVR}_{\text{FLOW}_{\text{SRTM}}}$ , in case of intermediate (Figure 5) to high (data not shown) amyloid levels.

**Sensitivity to CBF changes – The effect of noise.** Overall, effects of noise on the sensitivity of the different methods to CBF changes were minimal for full TACs (maximum difference: 1 percentage point (p.p.)), see Supplementary Figure 2). Furthermore, for interval TACs, more outliers and a larger sensitivity were observed at higher compared to lower noise levels.

**Sensitivity to CBF changes – Acquisition start time and duration.** Overall, later uptake times showed a decreased sensitivity to CBF changes for both tracers ([ $^{18}\text{F}$ ]flutemetamol:  $\chi^2 = 54$ ,  $p < 0.001$ , [ $^{18}\text{F}$ ]florbetaben:  $\chi^2 = 127$ ,  $p < 0.001$ ). Post hoc tests revealed the effect was not present for [ $^{18}\text{F}$ ]flutemetamol cortical changes. Furthermore, CBF increases resulted in a higher  $\text{SUV}_{\text{FLOW}}$ , while CBF decreases caused the opposite effect, except for [ $^{18}\text{F}$ ]flutemetamol cortical changes (Figure 6). Varying the duration of the uptake period

from 20 to 15 or 10 min provided essentially identical results for [ $^{18}\text{F}$ ]flutemetamol. With respect to [ $^{18}\text{F}$ ]florbetaben,  $\text{SUV}_{\text{FLOW}}$  calculated over 20 min showed significantly less CBF sensitivity compared with  $\text{SUV}_{\text{FLOW}}$  calculated over 10 min ( $p = 0.005$ ). With respect to  $\text{DVR}_{\text{FLOW}_{\text{RLOGAN}}}$ , there was a small effect of linearization start time with later start times (corresponding to shorter acquisitions) being less sensitive to CBF changes ([ $^{18}\text{F}$ ]flutemetamol:  $\chi^2 = 78$ ,  $p < 0.001$ , [ $^{18}\text{F}$ ]florbetaben:  $\chi^2 = 8$ ,  $p = 0.04$ ). More specifically, global and cortical CBF changes resulted in a small decrease in CBF sensitivity for later linearization times ([ $^{18}\text{F}$ ]flutemetamol:  $\chi^2 = 66$ ,  $p < 0.001$  and  $\chi^2 = 49$ ,  $p < 0.001$ , respectively; [ $^{18}\text{F}$ ]florbetaben:  $\chi^2 = 36$  and  $p < 0.001$ ,  $\chi^2 = 14$ ,  $p = 0.003$ , respectively). On the other hand, for [ $^{18}\text{F}$ ]florbetaben, cerebellar CBF changes resulted in a small increase in the models sensitivity ( $\chi^2 = 44$ ,  $p < 0.001$ ; Supplementary Figure 3).

## Discussion

The current simulation study assessed the effect of global and regional CBF changes on regional amyloid

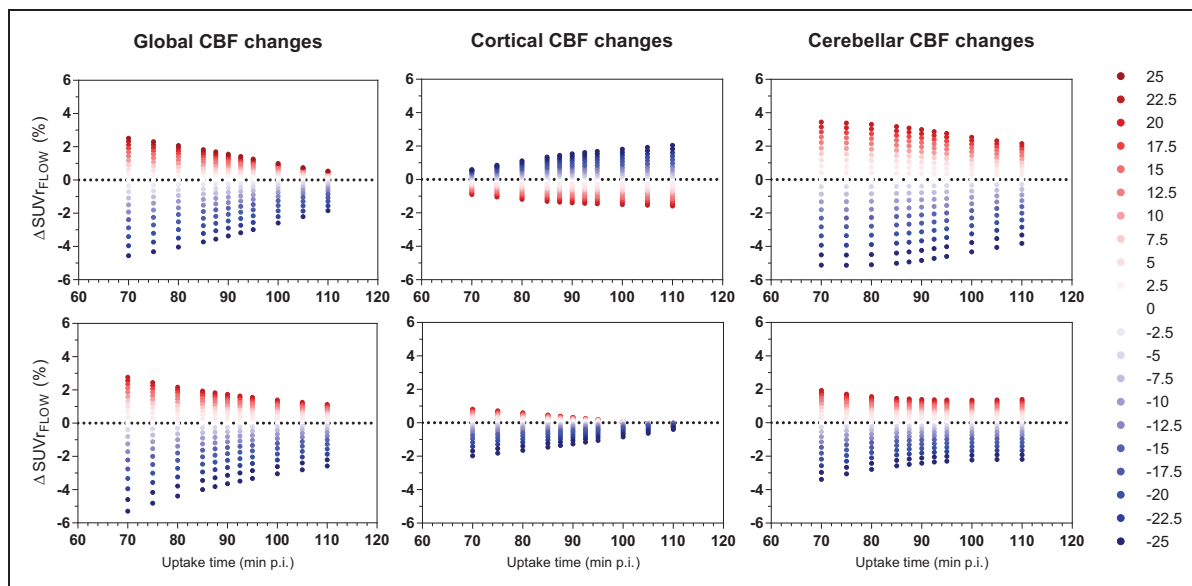


**Figure 6.** The effect of uptake time on sensitivity of SUVR to CBF changes. Upper row is [ $^{18}\text{F}$ ]flutemetamol and bottom row is [ $^{18}\text{F}$ ]florbetaben, depicted for intermediate amyloid ( $\text{DVR} = 1.400$  and  $\text{DVR} = 1.538$  for both tracers respectively) Red dots resemble CBF increases and blue dots CBF decreases.

quantification based on static, dynamic and dual-time-window scanning-protocols using reference tissue approaches for [ $^{18}\text{F}$ ]flutemetamol and [ $^{18}\text{F}$ ]florbetaben. The results of the present simulation study indicate that, compared with  $\text{DVR}_{\text{FLOW}_{\text{SRTM}}}$  and  $\text{SUVR}_{\text{FLOW}}$ ,  $\text{DVR}_{\text{FLOW}_{\text{RLOGAN}}}$  was less affected by changes in CBF for both [ $^{18}\text{F}$ ]flutemetamol and [ $^{18}\text{F}$ ]florbetaben. Furthermore, this sensitivity to CBF changes increased with increasing levels of amyloid. Finally, changes in the relative delivery rate  $R_1$ , obtained with SRTM, were highly correlated with simulated CBF changes.

The finding that  $\text{DVR}_{\text{FLOW}_{\text{RLOGAN}}}$  was robust against changes in CBF is in line with a previous study that found the same result for [ $^{11}\text{C}$ ]PiB<sup>5</sup> and this robustness may be due to the linearity of the model.<sup>24</sup> In contrast, SRTM was found to be somewhat more sensitive to changes in CBF for both tracers, which is in agreement with work of Bullich et al.<sup>7</sup> Their findings differ from the results reported here, in that they reported a slightly higher sensitivity of SRTM to cortical and a lower sensitivity to global CBF changes. This discrepancy may be attributed to differences in simulation design, the different cortical composite region and differences in fitter settings (such as parameter boundary values) between the studies.<sup>7,22</sup> In the present study, parameter boundary values were optimised to prevent fit parameters from becoming undetermined (i.e.  $k_2$  and  $BP_{\text{ND}}$ ), in particular for lower levels of amyloid.

The finding that  $\text{DVR}_{\text{FLOW}_{\text{SRTM}}}$  is sensitive to changes in CBF is probably due to the fact that the assumptions underlying SRTM are violated for both

tracers, i.e. the requirement that tracer kinetics are well described by a one-tissue compartment model in both the target and reference tissue.<sup>25</sup> More specifically, for both tracers the target and reference tissue kinetics have been shown to be better described by a two-tissue compartment model.<sup>3,21</sup> In contrast, RLogan does not assume any specific number of target tissue compartments, robustly estimating  $\text{DVR}_{\text{FLOW}}$  independent of the underlying compartmental separation. Furthermore, most outliers were present for interval compared to full TACs (outliers interval TACs: [ $^{18}\text{F}$ ]flutemetamol: 91.67%, [ $^{18}\text{F}$ ]florbetaben: 66.67%). These outliers were only observed for  $\text{DVR}_{\text{FLOW}_{\text{SRTM}}}$  and in particular for TACs corresponding to low amyloid levels.

With respect to  $\text{SUVR}_{\text{FLOW}}$ , effects of CBF changes were relatively small for both tracers (see Figures 3 and 4, maximum 5.1 and 6.1% for [ $^{18}\text{F}$ ]flutemetamol and [ $^{18}\text{F}$ ]florbetaben, respectively). However, SUVR's sensitivity to global CBF changes increased for higher amyloid levels, as also seen for the other models. A comparable finding has been reported for [ $^{18}\text{F}$ ]florbetapir, where amnesic MCI and AD subjects showed higher CBF sensitivity compared to controls, for large CBF decreases ( $-40\%$ ).<sup>18</sup> The maximum change in  $\text{SUVR}_{\text{FLOW}}$  was within the maximum reported change for other amyloid tracers that assessed slightly more extreme flow variations.<sup>5,18</sup> In addition, the sensitivity of  $\text{SUVR}_{\text{FLOW}}$  to CBF changes was, as expected, dependent on acquisition start time, with later start times being more robust against CBF fluctuations, except

for [ $^{18}\text{F}$ ]flutemetamol cortical changes. For [ $^{18}\text{F}$ ]flutemetamol, the direction of the relation between sensitivity to CBF changes and acquisition start time was, although less pronounced, comparable with [ $^{11}\text{C}$ ]PiB findings. More specifically, for cortical CBF changes, an increased sensitivity was observed for later uptake-times, while this relationship was inverted for global changes.<sup>5</sup> These results suggest that imaging data acquired at expedited instead of delayed uptake times should be interpreted carefully, as a greater impact of CBF changes on SUV<sub>r</sub> is expected.

It is of interest to note that, in some cases, the confounding effects of perfusion changes were different between the two tracers. TACs were simulated using parameters derived from existing studies.<sup>20,21</sup> Although sample sizes of those studies were different, it is unlikely that this had an effect on the final results, as both datasets consisted of 50% AD patients and 50% healthy controls. The most likely explanation for these differences in results is the difference in tracer kinetics of the two tracers, which can be deduced from the rate constants used for the simulations (Table 1). As mentioned above, reference tissue kinetics of both tracers were best described by including a second compartment, thereby violating the assumptions of a reference tissue model to some degree. More specifically, individual  $k_3$  and  $k_4$  parameters, as well as their ratio, differed between both tracers. This, in combination with differences in target tissue kinetics, could explain the observed differences between both tracers, which were most pronounced for SRTM, a model that assumes single tissue kinetics in both target and reference tissues. In other words, the difference in sensitivity to perfusion changes between both tracers is most likely due some degree of violation of underlying model assumptions, which may be different for the two tracers.

For both tracers, strong relationships ( $R^2 \geq 0.95$ ) were observed between SRTM-derived  $R_1$  changes and simulated changes in CBF. This finding was in agreement with the high correlation observed between SRTM-derived  $R_1$  and  $^{15}\text{O}$ - $\text{H}_2\text{O}$  PET, reported by a combined  $^{15}\text{O}$ - $\text{H}_2\text{O}$  PET and [ $^{18}\text{F}$ ]florbetapir study.<sup>16</sup> More specifically, it suggests that for both [ $^{18}\text{F}$ ]flutemetamol and [ $^{18}\text{F}$ ]florbetaben,  $R_1$  could be used as a proxy for measuring CBF.

Finally, the effect of noise (resembling regions of interest) on sensitivity to CBF changes for  $\text{DVR}_{\text{FLOW,RLOGAN}}$ ,  $\text{DVR}_{\text{FLOW,SRTM}}$  and  $\text{SUV}_{\text{FLOW}}$  was limited across amyloid levels. The effect of noise corresponding to a voxel level needs further validation, preferably using parametric imaging data.

As mentioned before, the main goal of this work was to assess the effect of global and regional CBF changes on regional amyloid quantification for [ $^{18}\text{F}$ ]flutemetamol and [ $^{18}\text{F}$ ]florbetaben studies. Overall, a maximum

CBF-induced change in amyloid outcome measure of 13.4% (SRTM) was observed across methods. However, it must be noted that the evaluated range of CBF changes was more extreme than the change one would typically expect during the timespan of a clinical trial or longitudinal study from an ageing or early AD perspective. On the other hand, in late AD stages, the CBF changes may be larger and drugs may also exert effects on CBF.<sup>12,13,15</sup> Although the exact size of the effect is unknown for many drugs, the effect of regularly used substances such as caffeine and nicotine ranges from  $-22$  to  $+25\%$ .<sup>28,29</sup> Therefore, besides the effect of drugs or stimulants, effects of CBF changes on  $\text{DVR}_{\text{FLOW}}$  and  $\text{SUV}_{\text{FLOW}}$  will likely be smaller than the effects reported in the present study.

The present results suggest that if large changes in amyloid load are to be expected, the possible confounding effects due to changes in perfusion are likely to be insignificant, obviating the need for a dynamic scanning protocol. However, in drug development studies, the drug may have unknown effects on perfusion, which must be well understood prior to implementation of simplified methods based on a static scanning protocol. This is especially relevant in secondary prevention trials, where measured changes in amyloid load may be small. In those cases, a dynamic or dual-time-window protocol should be used to assess whether changes in perfusion have occurred and to estimate their magnitude. Based upon this information, it can be decided whether a static protocol is sufficient or a dynamic protocol is needed to address a specific clinical or research question. Finally, it should be noted that a dynamic or dual-time-window scanning protocol also can provide a measurement of relative perfusion, which may be an additional relevant source of information. It should be noted that an exhaustive assessment of additional sources of bias was outside the scope of the present study. However, it is known from previous studies that SUV<sub>r</sub> typically shows a positive bias, while RLogan tends to underestimate the gold standard, and these intrinsic biases challenge the pooling of data from different methods.<sup>5,7,20,21</sup> Moreover, other factors such as image contrast and test-retest reliability may play a role when deciding on the method of choice for analysing data.<sup>6</sup> This implies that additional research, in particular test-retest and parametric imaging studies, is warranted.

Finally, given that the linear model (RLogan) outperformed the non-linear model (SRTM) with respect to robustness against CBF changes, one could conclude that SRTM is not the optimal model for describing the tracer's kinetics. Alternatively, a linearised form, basis function implementation of SRTM (RPM)<sup>30</sup> could be evaluated, which has shown improved performance,

especially for noisy data, compared to the original implementation of SRTM for [ $^{18}\text{F}$ ]flutemetamol.<sup>20</sup> The present study focussed on data corresponding to a region of interest level. As a next step, future studies could validate the application of parametric methods, such as RPM and SRTM2,<sup>31</sup> against the present results. The implementation of these methods (for example RPM's basis function settings) would ideally be validated using imaging data.

## Conclusion

RLogan was least affected by changes in cerebral blood flow and is therefore, at least within this context, the preferred method for regional amyloid quantification of [ $^{18}\text{F}$ ]flutemetamol and [ $^{18}\text{F}$ ]florbetaben. The same data could be analysed again using SRTM in order to determine the relative rate of delivery  $R_1$ , which showed good correlation with CBF. Finally, in most cases, effects of CBF changes on SUVr were relatively small, in particular for later uptake-times.

## Funding

The author(s) disclosed receipt of the following financial support for the research, authorship, and/or publication of this article: the project leading to this application has received funding from the Innovative Medicines Initiative 2 Joint Undertaking under grant agreement No 115952. This Joint Undertaking receives the support from the European Union's Horizon 2020 research and innovation programme and EFPIA <http://www.imi.europa.eu>. JDG holds a 'Ramón y Cajal' fellowship (RYC-2013-13054) from the Spanish Ministry of Science, Innovation and Universities.

## Acknowledgements

The authors would like to thank AMYPAD for all support and in particular prof. Frederik Barkhof for facilitating this research. In addition, we would like to thank Christopher Foley from GE for his feedback and the staff of the department of Nuclear Medicine, University of Leipzig for skilful acquisition and analyses of the [ $^{18}\text{F}$ ]florbetaben data during the clinical development.

## Authors' contributions

FH, MY, ILA, JDG, RB and AAL contributed to the concept and design of the study. SB, and KH provided the data. FH and MY contributed to the data analysis. FH, MY, ILA, KH, JDG, SB, RB and AAL contributed to the interpretation of the data. Technical or material support was provided by MY, SB and KH. FH, MY, ILA, and AAL drafted the manuscript. FH, MY, ILA, KH, JDG, SB, RB and AAL read, critically reviewed, and approved the manuscript.

## Availability of data and materials

The data generated in this simulation study are included in this article (and its supplementary materials) or can be made available upon reasonable request. Any requests regarding data received from GE Healthcare and Life Molecular Imaging GmbH can be directed towards those companies.

## Declaration of conflicting interests

The author(s) declared the following potential conflicts of interest with respect to the research, authorship, and/or publication of this article: SB is employed by Life Molecular Imaging GmbH. All other authors declare that they have no conflict of interest.

## ORCID iDs

Fiona Heeman  <https://orcid.org/0000-0001-7769-8329>  
Kerstin Heurling  <https://orcid.org/0000-0001-8497-9612>

## Supplemental material

Supplemental material for this article is available online.

## References

1. Jack CR, Knopman DS, Jagust WJ, et al. Hypothetical model of dynamic biomarkers of the Alzheimer's pathological cascade. *Lancet Neurol* 2010; 9: 119–128.
2. Mallik A, Drzezga A and Minoshima S. Clinical amyloid imaging. *Semin Nucl Med* 2017; 47: 31–43.
3. Nelissen N, Van Laere K, Thurfjell L, et al. Phase 1 study of the Pittsburgh compound B derivative 18F-flutemetamol in healthy volunteers and patients with probable Alzheimer disease. *J Nucl Med* 2009; 50: 1251–1259.
4. Carson RE, Channing MA, Blasberg RG, et al. Comparison of bolus and infusion methods for receptor quantitation: application to [ $^{18}\text{F}$ ]cyclofoxy and positron emission tomography. *J Cereb Blood Flow Metab* 1993; 13: 24–42.
5. van Berckel BNM, Ossenkoppele R, Tolboom N, et al. Longitudinal amyloid imaging using 11C-PiB: methodologic considerations. *J Nucl Med* 2013; 54: 1570–1576.
6. Yaqub M, Tolboom N, Boellaard R, et al. Simplified parametric methods for [ $^{11}\text{C}$ ]PIB studies. *Neuroimage* 2008; 42: 76–86.
7. Bullich S, Barthel H, Koglin N, et al. Validation of non-invasive tracer kinetic analysis of 18F-florbetaben PET using a dual-time-window acquisition protocol. *J Nucl Med* 2018; 59: 1104–1110.
8. Heeman F, Yaqub M, Lopes Alves I, et al. Optimized dual-time-window protocols for quantitative [ $^{18}\text{F}$ ]flutemetamol and [ $^{18}\text{F}$ ]florbetaben PET studies. *EJNMMI Res* 2019; 9: 32.
9. Frackowiak RS. Measurement and imaging of cerebral function in ageing and dementia. *Prog Brain Res* 1986; 70: 69–85.
10. Pantano P, Baron JC, Lebrun-Grandié P, et al. Regional cerebral blood flow and oxygen consumption in human aging. *Stroke* 1984; 15: 635–641.

11. Bremmer JP, van Berckel BNM, Persoon S, et al. Day-to-day test-retest variability of CBF, CMRO<sub>2</sub>, and OEF measurements using dynamic 15O PET studies. *Mol Imaging Biol* 2011; 13: 759–768.
12. Mosca F, Bray M, Lattanzio M, et al. Comparative evaluation of the effects of indomethacin and ibuprofen on cerebral perfusion and oxygenation in preterm infants with patent ductus arteriosus. *J Pediatr* 1997; 131: 549–554.
13. de Jong DLK, de Heus RAA, Rijpma A, et al. Effects of nilvadipine on cerebral blood flow in patients with Alzheimer disease: a randomized trial. *Hypertension* 2019; 74: 413–420.
14. Postiglione A, Lassen NA and Holman BL. Cerebral blood flow in patients with dementia of Alzheimer's type. *Aging* 1993; 5: 19–26.
15. Alegret M, Cuberas-Borrós G, Vinyes-Junqué G, et al. A two-year follow-up of cognitive deficits and brain perfusion in mild cognitive impairment and mild Alzheimer's disease. *J Alzheimers Dis* 2012; 30: 109–120.
16. Ottoy J, Verhaeghe J, Niemantsverdriet E, et al. 18F-FDG PET, the early phases and the delivery rate of 18F-AV45 PET as proxies of cerebral blood flow in Alzheimer's disease: Validation against 15O-H<sub>2</sub>O PET. *Alzheimers Dement* 2019; 15: 1172–1182.
17. Sojkova J, Beason-Held L, Zhou Y, et al. Longitudinal cerebral blood flow and amyloid deposition: an emerging pattern? *J Nucl Med* 2008; 49: 1465–1471.
18. Ottoy J, Verhaeghe J, Niemantsverdriet E, et al. A simulation study on the impact of the blood flow-dependent component in [18F]AV45 SUVR in Alzheimer's disease. *PLoS One* 2017; 12: e0189155.
19. Chen YJ, Rosario BL, Mowrey W, et al. Relative 11C-PiB delivery as a proxy of relative CBF: quantitative evaluation using single-session 15O-water and 11C-PiB PET. *J Nucl Med* 2015; 56: 1199–1205.
20. Heurling K, Buckley C, Van Laere K, et al. Parametric imaging and quantitative analysis of the PET amyloid ligand [(18F)]flutemetamol. *Neuroimage* 2015; 121: 184–192.
21. Becker GA, Ichise M, Barthel H, et al. PET quantification of 18F-florbetaben binding to  $\beta$ -amyloid deposits in human brains. *J Nucl Med* 2013; 54: 723–731.
22. Yaqub M, Boellaard R, Kropholler MA, et al. Optimization algorithms and weighting factors for analysis of dynamic PET studies. *Phys Med Biol* 2006; 51: 4217–4232.
23. Morris ED, Endres CJ, Schmidt KC, et al. Kinetic modeling in positron emission tomography. In: Wernick MN and Aarsvold JN (eds) *Emission Tomography: The Fundamentals of PET and SPECT*. Amsterdam: Elsevier Inc., 2004, pp. 499–540.
24. Logan J, Fowler JS, Volkow ND, et al. Distribution volume ratios without blood sampling from graphical analysis of PET data. *J Cereb Blood Flow Metab* 1996; 16: 834–840.
25. Lammertsma AA and Hume SP. Simplified reference tissue model for PET receptor studies. *Neuroimage* 1996; 4: 153–158.
26. Kruskal WH and Wallis WA. Use of ranks in one-criterion variance analysis. *J Am Stat Assoc* 1952; 47: 583–621.
27. Tukey JW. *Exploratory data analysis*. Reading, MA: Addison-Wesley Pub. Co., <http://www.gbv.de/dms/bowker/toc/9780201076165.pdf> (1977, accessed 27 August 2019).
28. Lunt MJ, Ragab S, Birch AA, et al. Comparison of caffeine-induced changes in cerebral blood flow and middle cerebral artery blood velocity shows that caffeine reduces middle cerebral artery diameter. *Physiol Meas* 2004; 25: 467–474.
29. Wennmalm A. Effect of cigarette smoking on basal and carbon dioxide stimulated cerebral blood flow in man. *Clin Physiol* 1982; 2: 529–535.
30. Gunn RN, Lammertsma AA, Hume SP, et al. Parametric imaging of ligand-receptor binding in PET using a simplified reference region model. *Neuroimage* 1997; 6: 279–287.
31. Wu Y and Carson RE. Noise reduction in the simplified reference tissue model for neuroreceptor functional imaging. *J Cereb Blood Flow Metab* 2002; 22: 1440–1452.